

GT2018-76994

AN EXPERIMENTAL STUDY OF USING VORTEX GENERATORS AS TIP LEAKAGE FLOW INTERRUPTERS IN AN AXIAL FLOW TURBINE STAGE

Veerandra C. Andichamy

Gohar T. Khokhar

Cengiz Camci

The Pennsylvania State University, Dept. of Aerospace Engineering
Turbomachinery Aero-Heat Transfer Laboratory
University Park, PA, 16802

ABSTRACT

The flow leaking through the gap between rotor blade tips and casing surface in a turbine stage is an important source of energy loss. The current study uses a new concept named as **Tip Leakage Interrupters (TLI)** to mitigate some of the adverse effects of the tip leakage flows and improve the efficiency of an axial turbine stage. The TLIs are a system of vortex generators attached onto the suction side of the turbine blade tip. The TLI design was developed in a proof of concept effort and they operate by inducing controlled vortical structures originating from strategically shaped/oriented multiple and sub-miniature vortex generators. These induced vortical structures, when properly interact with the tip leakage vortex reduce the damaging aerodynamic effects of the leakage flow. The TLIs in this investigation were mounted near the suction side corner of turbine blade tips rotating in a single-stage cold-flow turbine facility. In this investigation, three different parameters such as the mounting location of TLI on the airfoil tip region, the number of TLIs mounted and the specific orientation of TLI were varied. The TLI mounted near the minimum pressure point on the suction side of the blade generated the largest vortical structure that is counter rotating to the leakage vortex system and hence had the greatest effect in reducing the strength of the leakage vortex. Adding more TLIs on the blade suction surface was found to improve the tip leakage mitigation effort. The study showed that changing the specific orientation of the TLI with respect to the incoming flow drastically changes the rotational direction of the vortex it generates and its nature of interaction with the leakage vortex.

NOMENCLATURE

A	Reference Area in spanwise distribution of DeltaC _p plot
AFTRF	Axial Flow Turbine Research Facility
c	Rotor axial chord-length at tip = 0.0864 m
C _p	Total pressure coefficient C _p =ΔP ₀ /0.5ρU _m ²
C _{p25%}	Total pressure coefficient at 25% of blade-span
C _{p34%}	Total pressure coefficient at 34% of blade-span
CW	Clockwise
CCW	Counter clockwise
CMOS	Complementary Metal Oxide Semiconductor
Delta C _p	Passage averaged C _p of a passage – average of (Passage averaged C _{p25%} to C _{p340%}) of the passage
DC	Direct Current
DTP	Dynamic Total Pressure (probe)
E ³	Energy Efficient Engine
ECB	Eddy Current Brake
FOM	Figure of Merit
GUI	Graphics User Interface
h	Rotor blade height = 0.123 m
HP	High Pressure
k	Casing surface roughness
N	Rotor speed (RPM)
NGV	Nozzle Guide Vane
P _{atm}	Atmospheric pressure
ΔP	Pressure measured by Validyne transducer
ΔP ₀	Total pressure drop measured by DTP probe
r _m	Rotor radius at mid-span
t	Rotor tip clearance height
T	Total temperature

TC	Relative tip clearance $TC = t/h$
TLI	Tip Leakage Interrupter
U_m	Mid-span rotor speed, $U_m = \omega \cdot r_m$
ω	Angular velocity of the rotor blade
ρ	Density of air

INTRODUCTION

In a turbine-stage maintaining a tight gap between the rotor blade tip and outer casing surface is essential for maximizing the aerothermal performance of the turbine blades. However, the tip clearance gap cannot be reduced below a certain height, as it would result in mechanical complications such as rubbing of blades and casing surface. The presence of this gap facilitates the flow to leak from the pressure side to the suction side of the blade tip. This leakage flow interacts with hot gas side flow features near the suction side of the blade and swirls to form a flow system called tip leakage vortex. Boyle et al. [1] showed that even though the tip gap takes up a small physical space in a turbine stage and only negligible mass (compared to the core flow) flow passes through it, the losses developed by it accounts for over 30% of overall aerodynamic losses in a turbine stage. The unsteadiness and the momentum deficit introduced by the tip leakage flow also propagates to the subsequent turbine stages and thereby decreases the stage efficiency further. In addition to aerodynamic loss generation, tip leakage flows also unloads the blade tip, making it inefficient and unable to turn the incoming flow. They measurably reduce the work extraction ability of the tip section. Glassman [2] showed that often the blade unloading is not confined only to the blade tip but also propagates to other spanwise locations of the blade, decreasing the overall efficiency of the blade.

The tip leakage flow generate losses at two different regions. First is the losses generated inside the tip gap and the second is the losses generated by the mixing of leakage flow with main flow. Bindon [3] showed that the losses in the tip gap region are developed due to various flow features such as secondary losses and end wall effects near the blade tip, flow features due to separation bubble in the tip gap and formation of a shear layer in the gap. To quantify the losses due to mixing of leakage flow and the mainstream flow Denton [4] proposed a simple loss model by treating the mixing of leakage flow and the main flow as a cross flow in jet stream. Even though this model is basic and cannot be used to find the absolute loss value of tip leakage flow, it is very helpful in determining the trends of the leakage loss. The region near the blade tip have undergone several modifications to reduce this aerodynamic loss in the turbine stage. A summary of some of these modifications are provided below.

Squealer tip cavities: For squealer blade tip a recirculatory flow is developed in the squealer cavity which acts as a barrier to the flow entering the tip gap. A study by Key et al. [5] shows that the squealer tips have about 10% less losses than flat tips. Several modifications to the squealer blade such as partial squealer were made to improve the blade performance.

Dey et al. [6] and Camci et al. [7] studied the effect of partial squealer where only specific portion of the blade tip had squealer rim type extensions. The results showed that the suction side squealer was more effective in reducing the leakage flow across the blade tip. This is because when the leakage flow meets with the suction side rim of the squealer cavity arrangement rolls up some of the leakage vortex in the central portion of the cavity. This vortex hinders the entry of the leakage flow into the tip gap of the suction side rim measurably reducing the leakage mass flow rate. Senel et al. [8] studied the influence of the squealer rim width and height in a parametric computational effort

Winglet or tip extensions: Winglets in airplane wings reduces the effect of wing tip vortices, similarly the winglets in turbine blades can be used to reduce the effect of tip leakage vortices. The winglet on the pressure side of a blade tip reduces the discharge coefficient of the leakage flow at the entrance region. In a set of rotating turbine rig experiments Dey et al. [9] showed that the suction side winglets are not as effective in reducing the leakage flow as the pressure side winglets. The pressure side extension on the blade tip acts as a barrier to the flow leaking to the tip gap region, and effectively reduces the mass flow rate of the leakage flow.

Leakage control via tip injection: Injecting coolant fluid in the tip gap is essential to reduce the thermal load on tip region surfaces. Rao et al. [10] found that by strategically injecting high momentum fluid into the tip gap from the blade tip platform, the mass flow rate and the momentum of the tip leakage vortex can be reduced. The injected fluid blocks the entry of the tip leakage flow and thus reduces the leakage mass flow rate. Rao and Camci [11, 12] also found that coolant fluid injection at about 80% of the blade axial chord on the tip platform provided better loss control.

Tip leakage control via casing treatments: In addition to blade tip, changes can be also made on casing surface to reduce the leakage mass flow rate. Rao et al. [13] studied the effect of casing surface roughness on tip leakage flow. The casing surface was roughened using sand papers of two different roughness ($k = 66 \mu m$ and $k = 141 \mu m$). The results obtained from this study showed that roughening the casing surface significantly reduced the leakage mass flow rate. This is due to the variation of the three-dimensional casing boundary layer and changes in the entrance condition of the tip gap. Gumusel [14] found that having curved casing patterns (somewhat like the camber of blade tip airfoil) on the casing surface measurably reduced the tip leakage loss in the system. A numerical investigation of the aerodynamic influence of circumferentially aligned grooves in the casing was performed by Kavurmacioglu et al. [15] and found that the deep circumferential grooves in the casing surface provided better aerodynamic performance than the shallow circumferential grooves.

In all the above studies the losses associated with tip leakage flows were controlled by reducing the leakage mass flow rate through the tip gap. The overall loss was reduced by reducing the loss generated inside the tip gap which then indirectly reduces the loss generated by mixing of leakage flow and the main stream. In the present study, the modification to the

blade tip region outside the tip gap is considered. The aim is not to reduce the leakage mass or to reduce the loss generated in the tip gap but to control the mixing loss generated by fluid emerging from the tip gap towards mainstream fluid near the suction side. The concept of “Tip leakage Interrupter-TLI” is explained in detail to counteract the damaging vortical flows of the tip leakage fluid.

Vortex generator flows: Conventional vortex generators operate by positioning them obliquely with respect to the local incoming airflow. This interaction of the approach flow and the vortex generator creates highly distinctive vortical structures downstream. As these stream-wise vortices bring more turbulent kinetic energy into the low momentum zones, the vortex generators are used in turbine blades to reduce the boundary layer separation on the suction side of the low-pressure turbine blades, in transition ducts or inlet channels. Bons et al. [16] used a linear turbine cascade to study the effect of pulsed vortex generator jets on to the flow separation on the suction side of a low-pressure turbine blade. High frequency solenoid feed valves were used to generate the pulsed jet flow. The results from the study showed elimination of boundary layer separation on the suction side and a reduction in the blade wake loss profile.

In addition to preventing boundary layer separation, vortex generators are also used to enhance the heat transfer rates in heat exchangers or cooling passages. Gokce et al. [17] showed that vortex generators embedded on the end-wall surface before the circular pin fins of a turbine coolant channel increased the heat transfer rates downstream of the pin fins by 10%. In a patent by Beeck et al. [18], vortex generators were inside the turbine blade squealer cavity to reduce the leakage flow exiting from the blade tip gap. The vortex generators were directly positioned on the bottom of the squealer cavity of the tip.

Current TLI concept definition: In this present investigation, the leakage flow related loss in the turbine stage is controlled by strategically placing the Tip Leakage Interrupters (TLIs) near the suction side corner of the blade tip airfoil (as shown in Fig. 1). The flow passing over the inclined edge of the TLI accelerates around the edge and generates a low pressure zone in the immediate downstream of the TLI's inclined edge. This pressure difference causes the flow to change direction and roll up into a vortical structure counter-rotating to the leakage vortex. Figure 2, illustrates a typical vortex generated by a TLI. The leakage vortex has high turbulence intensity as studied by Xiao et al. [19] and McCarter et al. [20] and mix more rapidly than the passage vortex. The tip leakage vortex system interacting with the induced TLI vortex is likely to reduce its strength as they both are counter rotating in nature. The number, the location and the orientation of TLIs are of critical importance for the effectiveness of TLIs.

Any surface modifications on suction surface near the blade tip, which obstructs the mainstream flow should result in increased local total pressure loss especially near the local high Mach number zones in HP turbines. However, the turbine blade tip region is already handicapped in terms of work generation. The proposed TLI designs should be designed such that they should not cause significant aerodynamic penalty in the work

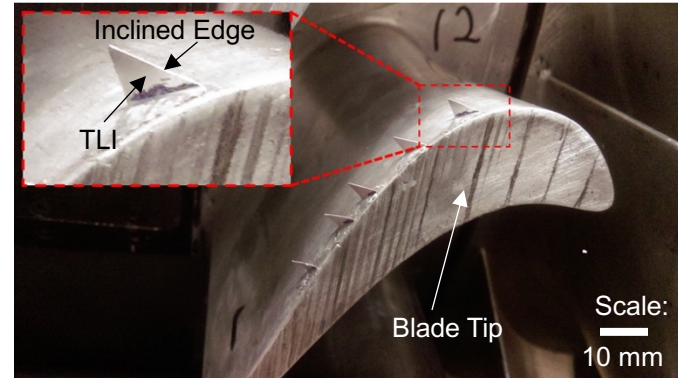


Figure 1: Five TLIs attached on the suction side corner of turbine blade tip

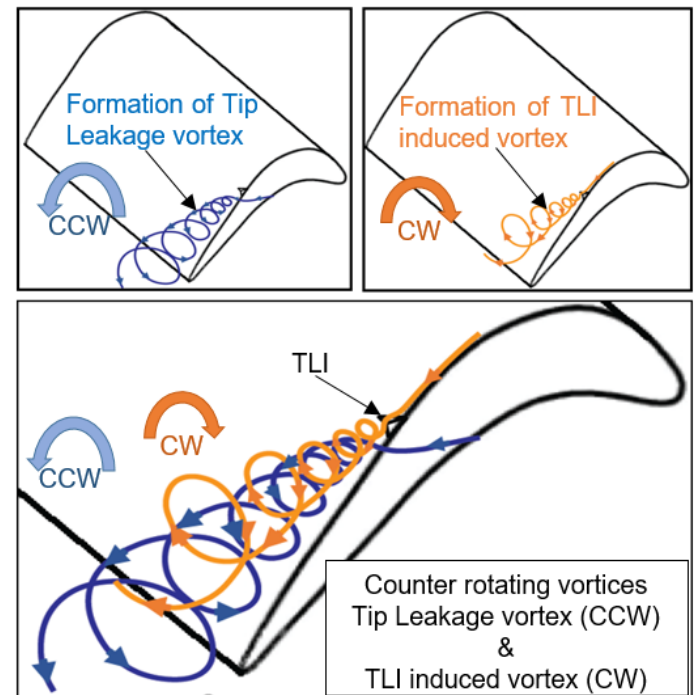


Figure 2: Interaction of the tip leakage vortex and the TLI induced vortex

output of the turbine. Sub-miniaturized TLI designs are essential. It is shown in this investigation that the damaging aerodynamic loss generation character of the tip vortex flow system can be positively influenced (reduced) by carefully sized and distributed TLI type vortex generators. In the current study, three different parameters such as the mounting location of TLIs on the airfoil tip region, the number of TLIs mounted on the blade tip and the specific orientation of the TLI were varied to study TLI's aerodynamic effect on the tip leakage vortex.

EXPERIMENTAL FACILITY AND PROCEDURE

Turbine Research Facility: The Axial Flow Turbine Research Facility (AFTRF) (Fig. 3) at the Pennsylvania State University is a low speed, large scale turbine rig running at 1330 RPM. A detailed report about this “cold flow turbine” facility is presented in Lakshminarayana, Camci, Halliwell and Zaccaria [21]. AFTRF HP turbine inlet is open to atmospheric pressure and temperature conditions. This open circuit facility with a single HP turbine stage is driven by four-stage axial flow fans connected in series. The fans can generate about 40 inches of water (9954 Pa) pressure drop throughout the stage in the suction blower mode. The loading distributions of the stage depicts the E³ design of NASA. An Eddy Current Brake (ECB) is used to absorb the shaft power generated in the stage, and to control the rotational speed of the rotor. Using ECB, the rotor RPM can be adjusted in an RPM range from 175 and 2000 and can be kept constant within ± 1 RPM. The inlet flow characteristics including the turbulence intensity in front of the NGV assembly are documented in [6, 7, 10, 21, 24].

There are 26 nozzle guide vanes and 29 rotor blades in this facility. The span of the rotor blade is $h=123\text{mm}$. The flow Reynolds number in the turbine stage is representative of a modern high-pressure turbine stage, [21, 22, and 23]. The NGV airfoils deflects the flow by 70° and guides it to the rotor blades. The rotor blades have a hub to tip ratio of 0.7317, which is similar to that of a high-pressure turbine stage. The absolute flow angle with respect to the axial direction at the exit of the rotor is 25.16° at the tip and 35.13° at the hub. The tip clearance distribution for all blades are presented in Table 1. It should be noted that the two blades having a tip clearance specification within $\pm 0.05\%$

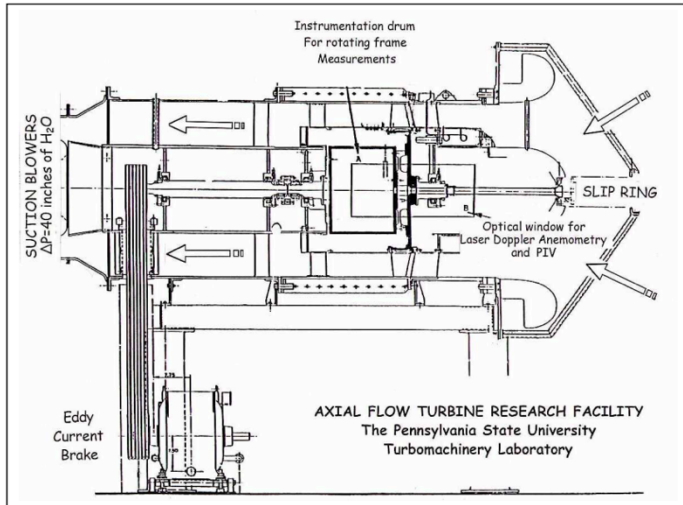


Figure 3: Cross sectional drawing of AFTRF, [21]

are considered to have the same tip clearance as they are within clearance measurement uncertainty of 2.5 mils (0.06mm). The four individual blades having the tip clearances of 0.78%, 0.80%,

0.81% and 0.83% are considered to have the same overall tip clearance.

Instrumentation: The performance of the turbine stage was monitored using K-type thermocouples, pitot-static probes and total pressure probes. The **Dynamic Total Pressure probe (DTP)** was used to measure phase-locked total pressure in the stationary frame of reference at 29.4% axial chord (25.4mm) downstream of rotor exit, as shown in Fig. 4. The measurement plane is normal to axis of rotation. It is aligned with the absolute velocity vector near the tip region at about 25.16° measured from the axial direction.

DTP probe and fast response pressure transducer: The DTP probe has a differential dynamic pressure transducer Endevco® 8507C-1 which was housed in a total pressure probe head to suit our experimental needs. The maximum diameter of the probe head facing the flow is 0.089 inches (2.26 mm). The cylindrical probe head has a square-cut tip design making the probe effectively operational in a wide pitch/yaw angle range. A pitch/yaw angle sensitivity study of the DTP probe done by Town [24] showed that the pressure data varied less than 1% of the nominal value within a yaw range of $\pm 10^\circ$. This yaw dependency is within the experimental error estimated for the C_p value obtained from DTP probe. The fast response pressure transducer used in DTP is shown in Fig. 5.

The Endevco® Model 8507C-1 is a rugged, miniature, high-sensitivity piezo-resistive pressure transducer with a full-scale output up to 300 mV. An active four-arm piezo-resistive bridge as shown in Fig. 5 is used to generate the raw data from the DTP transducer. This raw data is amplified and conditioned using an Endevco® model-136 DC differential voltage amplifier (200 Khz bandwidth) with auto-zero and shunt calibration. The DTP probe measures differential pressure with respect to the inlet atmospheric level. The reference port of the transducer is open to atmosphere.

The response time of this transducer is about 55 Khz for a differential pressure measurement range of ± 1 psi (± 6894.76 Pa). The DTP probe, due to its high transducer response time of 55 KHz can map the unsteady total pressure field at the rotor exit plane in a time accurate way. A protective mesh is used to cover the piezo-resistive transducer and it is attached to the DTP stem using high-temperature epoxy as shown in Figure 5. A linear probe traversing system with a stepper motor (Vexta), Stepper motor controller (Velmex VXM) and linear traverser (Velmex Unislide) was used to traverse the probe radially in the measurement plane at the rotor exit. The motors with their micro-stepping ability has better probe positional accuracy. Its fast response and fast movement reduces the time required to move to a specific measurement location. The radial traverser used in this experiment is mounted on the precision built and non-intrusive optical window opening.

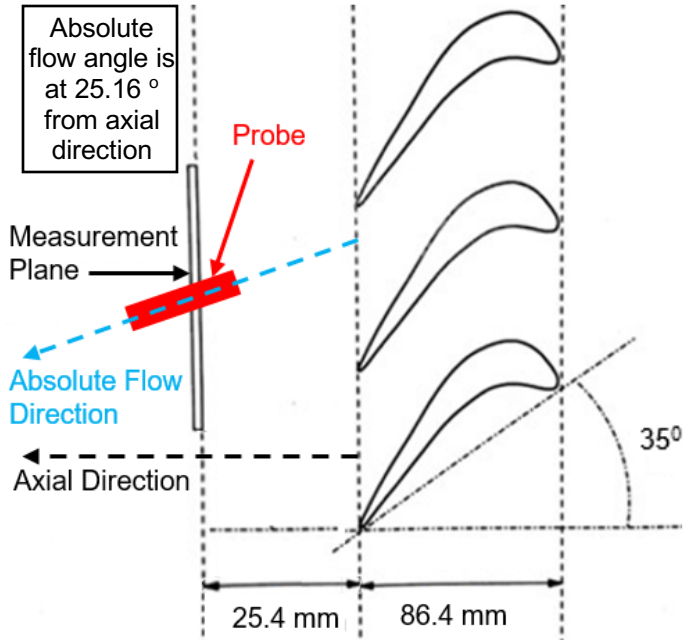


Figure 4: Alignment of DTP probe near blade tip

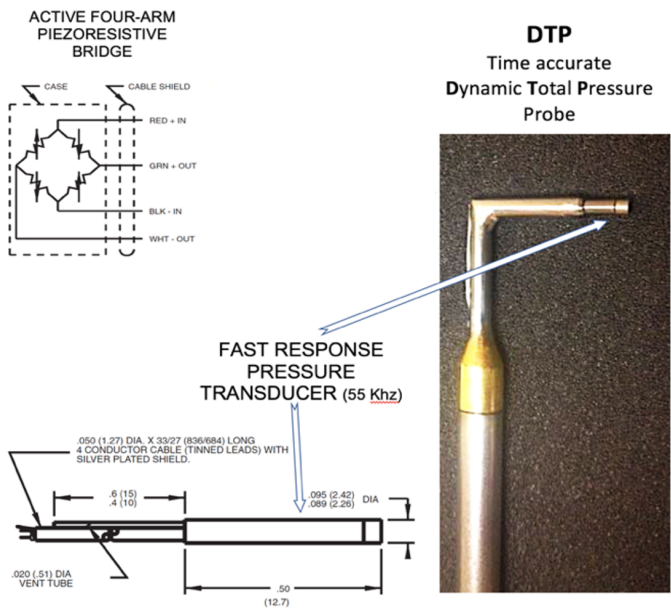


Figure 5: Fast response dynamic total pressure transducer and the time accurate Dynamic Total Pressure probe DTP

Data Acquisition: The Virtual Instrument (VI) setup in LabVIEW is used to control the data acquisition process. Data measured from the DTP probe is phase-locked to the rotor using a precision rotary encoder. The BEI-Sensors encoder attached to the turbine shaft has a rotating disk with 6000 equidistant precision-etched holes around its circumference. These holes are used to create 6000 TTL/CMOS pulses per revolution defining the starting of each measurement bin. The encoder output has two distinct signals, the first is one pulse-per-revolution and the

second one is 6000 pulses per revolution. The one pulse-per-revolution signal triggers the data system to collect DTP data while the 6000 pulses per revolution controls the data system to fill the bins of each revolution in a time accurate manner. As the encoder is directly attached to the rotating shaft, any slight change in the turbine RPM does not affect the relative angular position of each bin over 400 subsequent revolutions. The encoder guarantees an invariant angular position for each measurement in a specific bin. The inlet total pressure is at atmospheric level in AFTRF. The DTP probe uses Endevco transducer based differential dynamic total pressure measurements for the calculation of the total pressure coefficient C_p with atmospheric pressure as the reference pressure.

In a typical experiment, the DTP probe is moved from 97% blade-span to 25% blade-span with an increment of 1% blade-span. There is no measurement from hub to 25% blade-span because the specific effort is focused on the tip region. Due to the finite size of the probe and other mechanical limitations, the total pressure data from the last 3% of the blade height are not considered. The measurements in this region are dominated by probe wall proximity effects near the casing. The DTP probe is moved from one radial location to another by a linear traverser mechanism that is controlled by National Instruments PCI 6110-E multipurpose I/O board. Further details of the measurement system and the fast probe traverser is given in Town, Akturk and Camci, [22, 23]. The DTP collects 6000 phase-locked data points per revolution through 400 revolutions at each measurement location using the encoder system. The data used in this study are ensemble averages of the data from 400 subsequent rotations at each spanwise position. The data collected during a typical experimental run are processed via LabVIEW to calculate the flow properties and rotor performance. The processed data is stored and instantly displayed on the LabVIEW GUI screen. The data processing system is automated with an option of all the data being processed online. Town [24] gives a detailed description on the data system used in this study.

Experimental Uncertainty: The uncertainty analysis technique from Kline and McClintock [25] estimated that the total pressure coefficient C_p has 0.39% uncertainty. The measurement uncertainties of various sensors used in this study are given in Table 2. For all measurements at various spanwise positions, a fixed probe angle of 25.5° to the axial direction was maintained. From Town [22] it can be seen that the probe is insensitive to pitch/yaw angle variation within ±10°.

Design Details of the TLI: A schematic of TLI developed in this study is shown in Fig. 6. The TLI has two triangular sections, one is the base triangular section used to attach the TLI to the blade surface and the other is the "Vortex Generator" triangular section, used to generate the vortical structures. The "Vortex Generator" triangular section has three edges. First is the normal edge which is almost normal to the local blade surface, second is the inclined edge used to create vortices and the third is the base edge. The TLI is mounted near the blade tip suction side corner such that the base edge makes 45° locally to the blade tip section as shown in Fig. 7. Three different experiments called test A, test B and test C were performed using the TLIs. The test A was to

study the effect of mounting location of the TLI on the leakage vortex. In test B, the influence of the number of TLIs mounted on the blade surface was varied. In the last test C, the local orientation of the TLI with

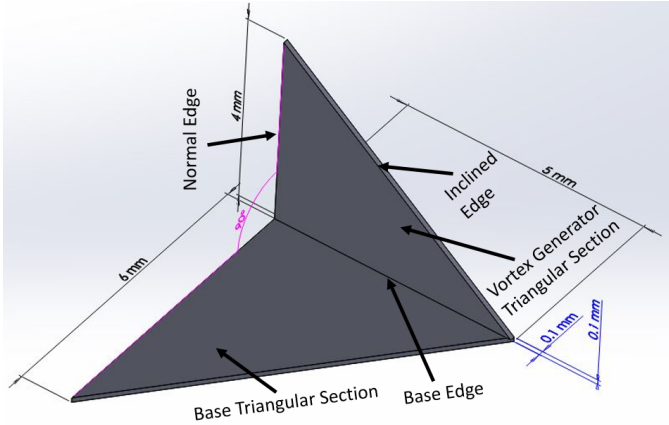


Figure 6: A typical Tip Leakage Interrupter (TLI)

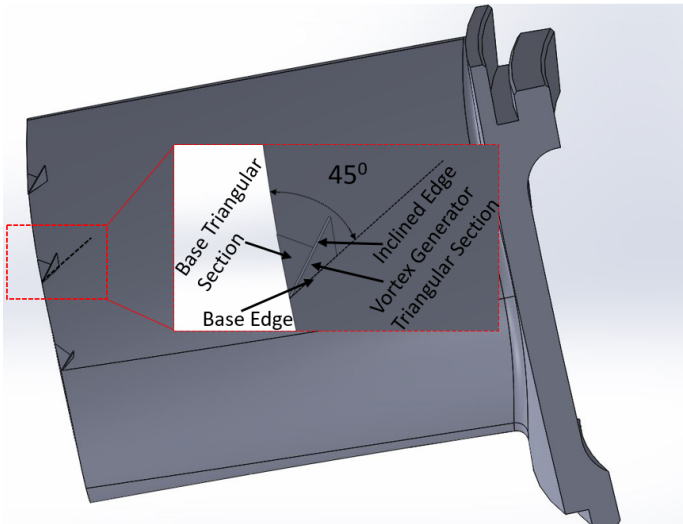


Figure 7: Tip Leakage Interrupter (TLI) blade design

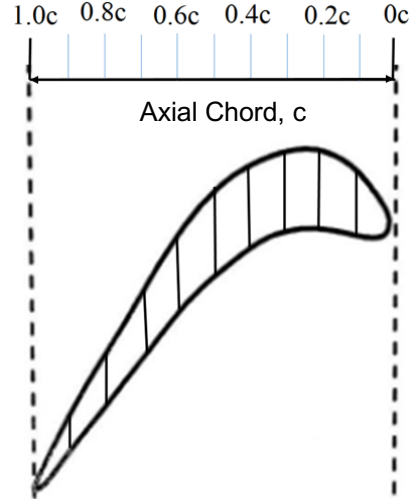


Figure 8: Ten equal segments of axial chord

respect to the blade tip was varied and its effect on the leakage vortex was studied. There are 29 blades in AFTRF numbered from 1 to 29. The passage between the two blades is also labeled with a "passage number" which is the same as the blade that has a pressure side in the passage. In all three experiments, TLI based modifications to the blade tip sections were implemented on blades with the same tip clearance. The details of the TLI based modifications made in the blade tip is given in Tables 3, 4 and 5. An AFTRF baseline blade with similar tip clearance and no tip modification was chosen as the reference blade. In test A, three different blades with similar tip clearance were selected. The three blades (blade 6, 8 and 14) were modified by attaching the TLI near the blade tip suction side corner at 40%, 65% and 75% of blade axial chord respectively measured from leading edge. The schematics of the axial chord

Table 1: The tip clearance values of all the blades

Blade No	Tip clearance (%) (t/h)	Blade No	Tip clearance (%) (t/h)	Blade No	Tip clearance (%) (t/h)
1	1.04	12	0.81	23	0.67
2	1.02	13	0.88	24	1.11
3	1.10	14	0.83	25	0.71
4	1.25	15	1.06	26	1.51
5	0.75	16	1.07	27	0.70
6	0.78	17	1.01	28	1.15
7	0.75	18	0.90	29	0.67
8	0.81	19	0.81		
9	0.81	20	0.80		
10	0.83	21	0.89		
11	0.81	22	0.68		

Table 2: The measurement uncertainty of the sensors used in this study

Parameter	Nominal Value	Uncertainty	Uncertainty (% of nominal value)
Validyne transducer, ΔP	7500 Pa	± 5 Pa	$\pm 0.067\%$
Dynamic pressure, ΔP_0	7500 Pa	± 8 Pa	$\pm 0.1067\%$
K-type thermocouple, T	300 K	± 0.2 K	$\pm 0.067\%$
Rotor Speed, N	1330 rpm	± 1 rpm	$\pm 0.075\%$
Atmospheric Pressure, P_{amp}	98700 Pa	± 100 Pa	$\pm 0.101\%$
Tip Clearance, t	1524 μm	63.5 μm	4.17%

locations on the blade is given in Fig. 8. Blade 20 was selected to be the reference blade. Similarly, for test B, three different blades (blades 8,10 and 12) were selected for the modification with blade 14 as a reference blade. Blade 8 had just one TLI, blade 10 had three TLIs and blade 12 had five TLIs mounted on the blade tip. In case of test C blade 6 had the five TLIs mounted at 45° to the blade tip section, and the blade 12 had the five TLIs mounted at 135° . The reference blade for this test is also blade 14.

EXPERIMENTAL RESULTS AND DISCUSSION

Contour Plots of C_p From Time Accurate and Ensemble Averaged DTP Probe:

As the main flow turns and progresses in the rotor passages, the total pressure is significantly reduced because of work extraction and the loss of mean kinetic energy of the flow due to viscous dissipation. In general, the most energy efficient region in a turbine flow field is the core flow and, the least efficient region is near the blade tip region. The overall aero loss level existing in the wake region and secondary flow zones are intermediate levels between the least

Table 3: The TLI mounting locations on the three chosen blades for test A

Test A	Blade	Blade	Blade	Blade
Position dependent	6	10	14	20 (Reference)
Tip Clearance (% t/h)	0.78	0.83	0.83	0.80
Location of TLI on suction side of the blade tip (% of axial chord)	40	65	75	---

efficient (tip vortex) level and the most efficient (core flow) level. The phase-locked unsteady total pressure for all 29 blade passages is shown in Fig. 9. The non-dimensional C_p value is

calculated using Eq. (1) and U_m is blade velocity at mid span ($\omega.r_m$). The numerator of Eq. (1) is generated by the fast response differential pressure transducer imbedded in DTP probe shown in Fig. 5. The non-dimensional pressure as a pressure coefficient is as follows:

$$C_p = \frac{\Delta P_{measured}}{\frac{1}{2} \rho U_m^2} \quad (1)$$

In Fig. 9, larger negative magnitude of C_p corresponds to lower total pressure in the measurement plane. The smaller negative magnitude of C_p corresponds to higher total pressure. The orange/red color in the spectrum represent region with less losses while the blue color in the spectrum represents the region with more losses in the flow field. The hub boundary layers are not shown in Fig. 9. The radial black lines represent the start and end of each passage. The dotted radial line in the inner circle indicates the mid line of the corresponding passage. The outer dotted circle represents the circle traversed by blade tip and the inner circle indicates the root of the blade attached to the hub. The number in black near the outer circle represents the blade passage number and the number in red represents its corresponding tip clearance value. Fig. 9, also gives high-resolution total pressure information about core flows, blade wakes and leakage vortices and end-wall flows present in each blade passage. In this approach, each blade passage can be individually assessed and passage to passage variations are clearly differentiated because of the ensemble averaged C_p data from the fast response DTP probe. The strong influence of the tip clearance gap (t/h) on the tip leakage vortex and its interaction with the upper passage vortex is clearly shown in 29 individual passages shown in Fig. 9.

Passage Averaged Delta C_p Plots: The passage averaged C_p value of a selected blade passage is calculated by taking an arithmetic average of C_p value at all angular positions within a blade passage for given span. The average is obtained along the pitch line of the specific passage chosen. There are 6000/29 measurement bins along one pitch distance. The passage averaged C_p plot of passage 6 is shown in Fig. 10. Due to the rotation of the hub at the specific axial position, the end-wall boundary layer in this region is skewed. In addition to hub end-wall boundary layer, the passage vorticity also affects the region near 25% blade-span.

Table 4: The TLI mounting locations on the three chosen blades for test B

Test B	Blade 8	Blade 10	Blade 12	Blade 14 (Reference)
Number dependent	8	10	12	14 (Reference)
Tip Clearance (% t/h)	0.81	0.83	0.81	0.83
Number of TLIs	1	3	5	0
Location of TLIs on Suction side of the blade tip (% of axial chord)	40	40, 65, 75	40, 55, 65 70, 75	---

The core of the flow is around 57% to 60% of blade-span, hence this region has the maximum passage averaged C_p value as shown in Fig. 10. From 60% to 70% of blade-span, passage averaged C_p decreases linearly—due to the secondary vortex effect. The non-linearity of the passage averaged C_p distribution in the region 70% to 85% blade-span is due to the mixing of secondary vortex and tip leakage vortex. Near the blade tip the lowest passage averaged C_p is at the 92% of blade-span. This is because the core of the leakage vortex is in this blade-span. The passage averaged C_p at the very end of the blade tip increases due to the influence of the casing surface. As this is a study on blade tip leakage flow, the part of the plot above 70% blade-span is the focus area.

The part of passage from 85% blade-span to 97% blade-span is as named as region 1, and the part from 70% blade-span to 85% blade-span is named as region 2. The passage averaged C_p trend in these two regions significantly depends on the blade tip modifications and resulting flow modifications.

Elimination of Bias Error from the Passage Averaged Total Pressure Coefficient: Figure 11 compares passage averaged C_p from four individual passages (6, 10, 14 and 20). All four passages have the similar tip clearance gap, t/h (0.78%, 0.83%, 0.83% and 0.80%)

Table 5: The TLI mounting locations on the three chosen blades for test C

Test C	Blade 6	Blade 12	Blade 14 (Reference)
Orientation dependent			
Tip Clearance (% t/h)	0.78	0.81	0.83
Orientation of TLIs with respect to the local blade tip (in degrees)	45	135	---
Location of TLI on Suction side of the blade tip (% of axial chord)	40, 55, 65 70, 75	40, 55, 65 70, 75	---

within its measurement uncertainty. They are supposed to exhibit very similar C_p distributions along the spanwise direction. The

passage averaged C_p distribution from four different passages from the same turbine run has an "observable/non-negligible" level of data shift. The passage averaged C_p distributions near the hub from all four passages with similar clearance should have similar magnitude. If there is some data scatter near the hub, this is because of possible non-negligible passage to passage variation of overall blade passage geometry. Slight passage to passage variations can be effectively removed by subtracting a "reference C_p " near the hub obtained from the passage of interest. The "reference C_p " here is the arithmetic average of 10 pitch wise (passage) averaged data points near the hub (i.e. from 25% to 34% of blade-span). By performing a subtraction from a C_p using a reference C_p value, the bias errors due to passage to passage variations of small magnitude are effectively removed. This approach tends to remove passage to passage variations from the actual C_p data effectively as shown in Fig. 12. The differentiated passage averaged C_p obtained by this definition is called the Delta C_p given by Eq. (2). Using Kline and McClintock [25] uncertainty analysis technique, the uncertainty of Delta C_p was estimated to be 0.55%.

$$\begin{aligned} \text{Delta } C_p, \text{passage } i &= (\text{passage average } C_p \text{ of passage } i) \\ &- \text{avg}(\text{passage averaged } C_{p25\%} \text{ to } C_{p34\%}) \text{ of passage } i \end{aligned} \quad (2)$$

Another benefit of subtracting a "reference C_p " from "actual C_p " is that it removes bias errors from DTP probe for identical measurements repeated on the same day or on different days. It is our observation that, even though the present day dynamic pressure transducers produce reasonably repeatable dynamic signals, it also inherently generates non-negligible DC signal shifts in identically repeated experiments. If one plots the DTP ensemble averaged signal along a pitch line at a selected span in many repeated (identical) experiments, the bias problem exhibits itself. It is always the case that the signals do not match within usually quoted experimental uncertainty band. If left uncorrected this signal bias could become a significant measurement error. However, a simple post-processing procedure applied to C_p measurements may help to eliminate a good portion of bias errors. Subtracting a "reference C_p " from "actual C_p " is a very productive operation to remove

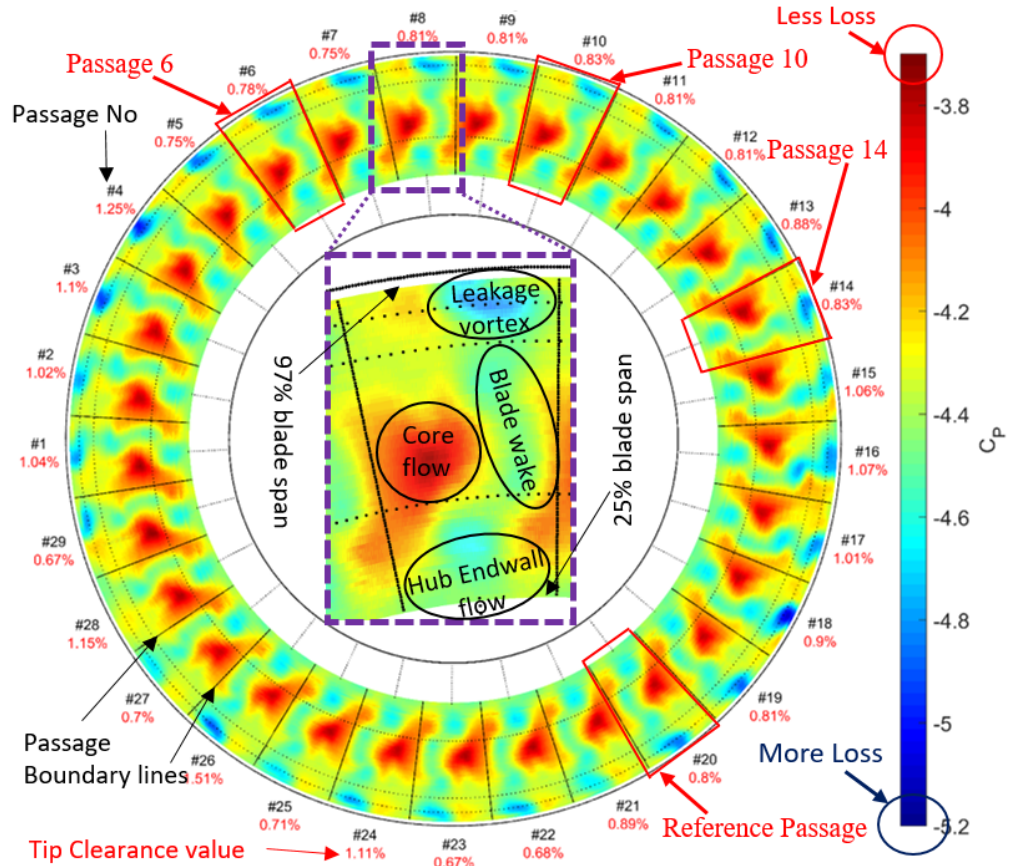


Figure 9: Total pressure contour plot of 29 passages in test A

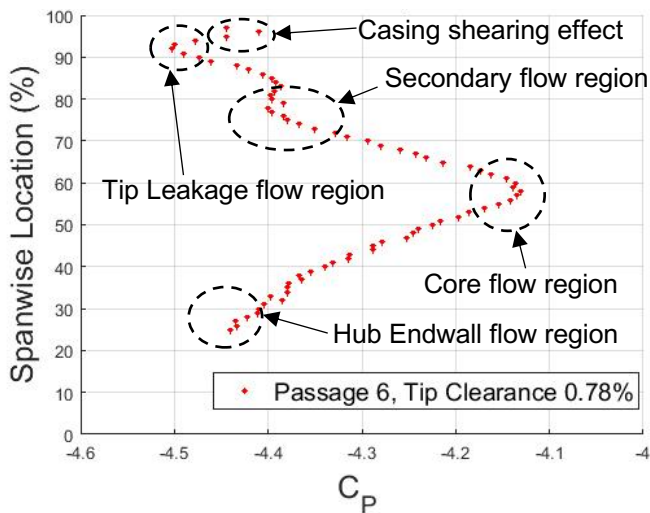


Figure 10: Passage averaged C_p spanwise distribution for passage 6

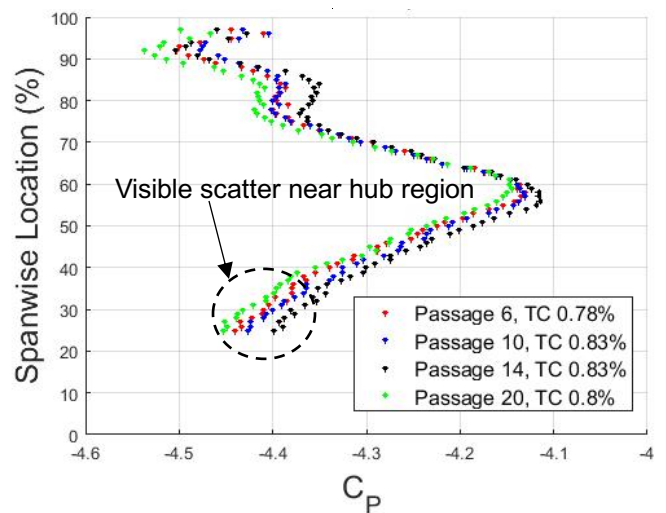


Figure 11: Passage averaged C_p spanwise distribution for passage 6, 10, 14 and 20

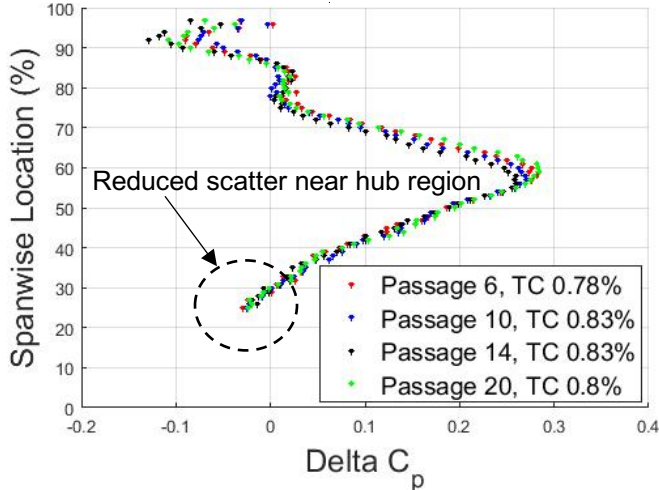


Figure 12: Span wise distribution of ΔC_p for passage 6, 10, 14 and 20

unwanted bias errors. It should be noted that the typical built-in internal temperature compensation circuitry of the current dynamic pressure transducers does not correct these bias errors. There may be many reasons for these bias errors. Such as mechanical/thermal cycling of the sensor assembly on the active face of the transducer, unsteady flow induced excitation of the transducer face, heat transfer to/from the sensor to probe housing, variations in sensor thermal stress levels may all cause the bias errors influencing the repeatability of typical DTP probes. The current method of removing "DTP signal bias" is also helpful in research programs where multiple experiments are executed over long-time periods. The method can also be applied in CFD efforts so that the DTP data from experiments can be easily assessed against CFD predictions. Figure 12 shows the result of using a "Delta C_p ". The bias errors are effectively eliminated and the consistency of results from the passages having the same clearance is markedly improved.

Figure of Merit: An effective comparison of turbine blade tip leakage mitigation schemes can be achieved by using a figure of merit. The Figure of Merit (FOM) of a blade is calculated by using the ΔC_p spanwise distribution of an individual blade. This ΔC_p distribution is then compared to a reference blade of the same experimental run. The FOM is useful in quantifying the aerodynamic effectiveness or ineffectiveness of a (novel) blade tip design from a blade tip having a conventional cylindrical tip running at the same resultant tip clearance. In the ΔC_p spanwise distribution plot, a vertical line called "Reference Line" is drawn at the maximum ΔC_p point of the reference blade passage (around 65% blade-span) as shown in Fig. 13. The area between the ΔC_p curve of the reference curve and the reference line from 97% to 70% of the blade-span is the

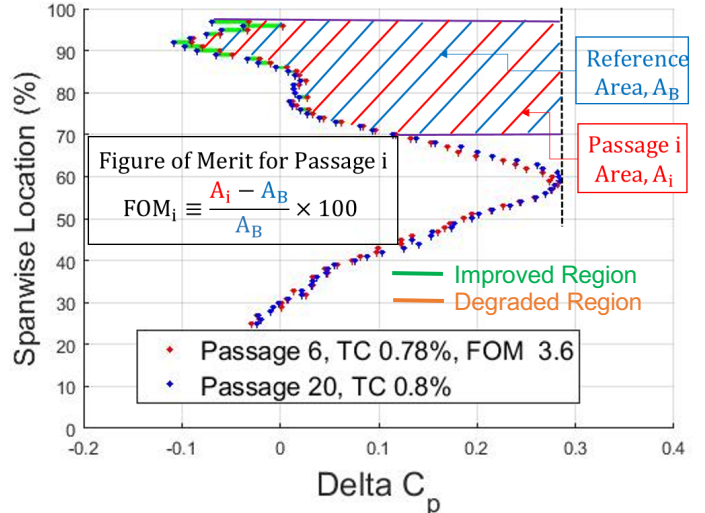


Figure 13: Figure of merit, FOM for passage 6 with passage 20 as reference passage

Reference Area, A_B . Similarly, the area between the ΔC_p curve of the desired passage and the reference line from 97% to 70% blade-span is Passage i Area, A_i . The Figure of Merit (FOM) definition is given as $(A_i - A_B)$ normalized by the reference area A_B , and multiplied by 100. The figure of merit for passage i, is given by Eq. (3). Details of the figure of merit calculation of passage 6 with respect to passage 20 is shown in Fig. 13. On the current ΔC_p axis, the horizontal shift of a data point to the left of the baseline data indicates increased total pressure loss (orange line). If the movement is to the right of the baseline data, the new concept has reduced loss (green line). The consideration of all green lines and orange lines from many spanwise locations in Fig. 13, indicates if the desired passage has less loss or more loss when compared to the reference passage. The figure of merit of passage 6 with respect to passage 20 is 3.7. As the passage 6 has positive FOM it has less loss in the passage than the reference passage (passage 20).

$$FOM_i \equiv \frac{A_i - A_B}{A_B} \times 100 \quad (3)$$

Test A: Figure 14, 15 and 16, compares the spanwise distribution of ΔC_p for passage 6, passage 10 and passage 14 with the reference passage (passage 20). The green and orange lines in the plot indicates the passage region positively and negatively influenced by the TLI respectively. Figure 14 shows that the TLI mounted at 40% axial chord reduces the losses in region 1 (97% to 85% blade-span) but it has very little effect on the other regions of the passage. The FOM of the passage 6 with respect to the reference passage 20 was calculated to be 3.6. The loss reduction in passage 6 is due to the vortical structure generated by the TLI in its downstream. The direction of rotation of these vortical flow system depends on the local angle of incidence of the flow with respect to the TLI. As the TLI is mounted at 45° to the local blade tip (Fig. 7) the vortex system it generates is in clockwise direction. The leakage vortex generated by the tip leakage flow is generally in the counter-clockwise direction. As

these two vortical systems are in opposite direction, the induced TLI vortex system on interaction with the tip leakage vortex reduces the overall strength of the leakage vortex. The schematics of induced vortex formation for blade 10 and its interaction with the leakage vortex is shown in Fig. 2.

Figure 15, shows that like passage 6, the losses in region 1 of passage 10 is also reduced due to the vortex induced by the TLI. A comparison of Fig. 14 and 15 shows that passage 10 have less loss than passage 6 in region 1. But in region 2 (85% to 70% blade-span), passage 10 have more loss compared to passage 6,

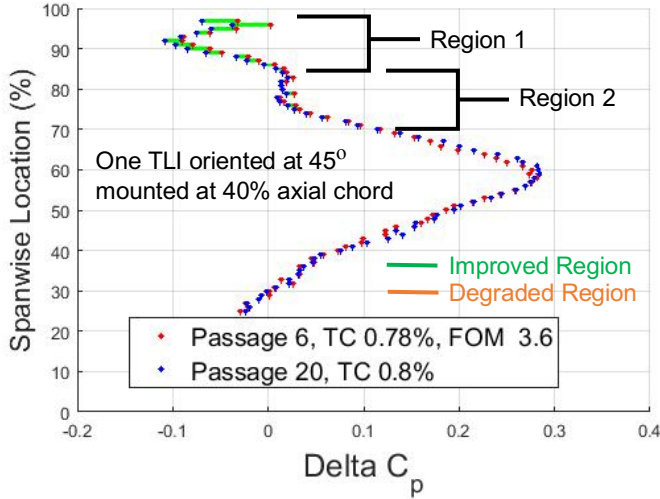


Figure 14: Spanwise distribution of ΔC_p for passage 6 with passage 20 as reference passage

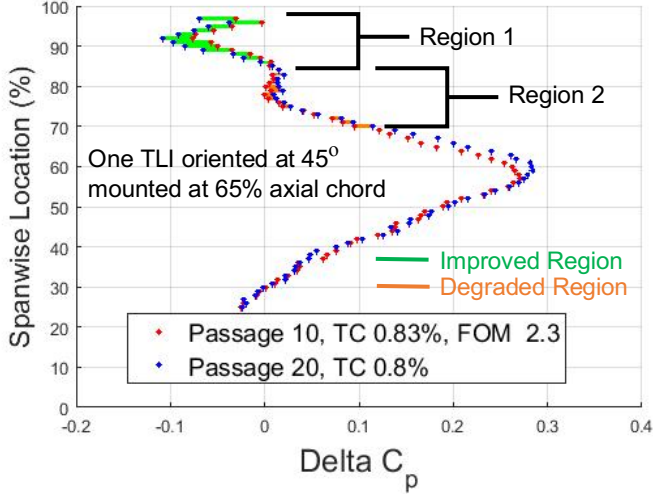


Figure 15: Spanwise distribution of ΔC_p for passage 10 with passage 20 as reference passage

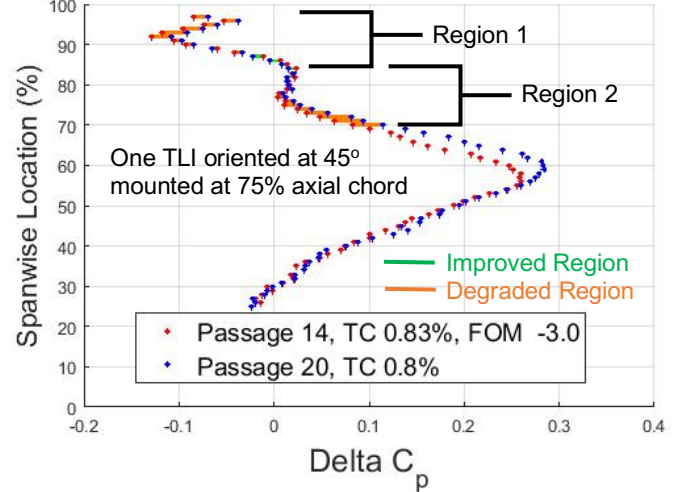


Figure 16: Spanwise distribution of ΔC_p for passage 14 with passage 20 as reference passage

which in turn increases the overall losses in passage 10. Hence, mounting TLI at 65% axial chord reduces the losses in region 1 but increases the losses in region 2. For untreated blade, the losses in region 1 are generated due to the tip leakage flow system, while the losses in region 2 are generated by the secondary flow (passage vortex). As they both are counter rotating, the strength of passage vortex in region 2 can be reduced by having stronger leakage vortex and vice-versa. In case of passage 10 the induced vortex generated by TLI reduces the strength of the leakage vortex, thus decreasing the losses in region 1. As the strength of the leakage vortex is reduced the influence of passage vortex is more in region 2 and thus increasing the losses in that region. Even though passage 10 have better flow characteristics compared to reference blade (as the FOM is 2.3) there is an increase in overall loss compared to passage 6.

In case of passage 14 more loss in the passage was developed due to addition of TLI onto the blade-tip. The orange lines in Fig. 16, shows the losses developed in region 1 and region 2 for passage 14. The losses generated in the passage was also indicated by the negative FOM value (-3.0) obtained for passage 14. In blade 14 as the TLI was mounted at 75% of axial chord, the leakage vortex developed before the TLI, overshadows and hinders TLI from generating vortical structures (as shown in Fig. 17). The TLI on the blade tip does not generate a vortex system to counteract the leakage vortex. This configuration acts as a barrier to the incoming flow and introduces additional losses in the system. Hence mounting TLI at 75% of axial chord in the blade tip measurably increased the losses generated in the passage and results in a negative FOM value.

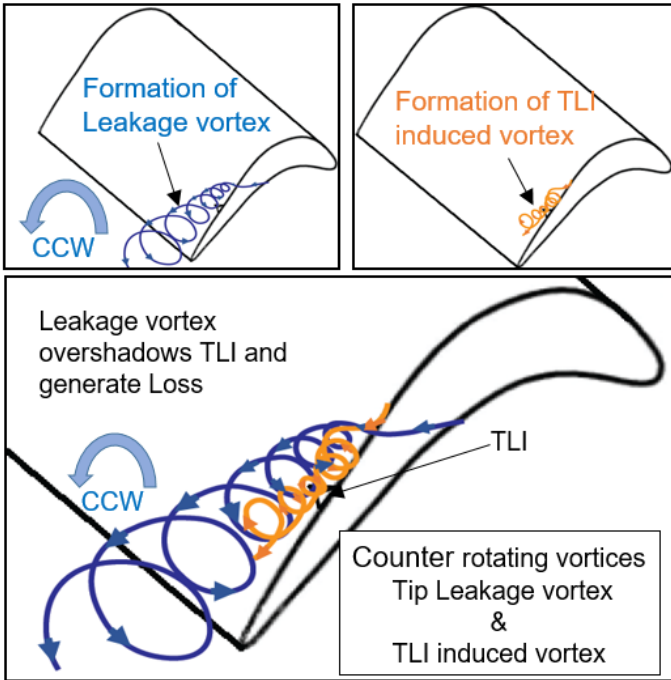


Figure 17: Interaction of the Tip leakage vortex and the TLI induced vortex in the blade 14

Results from Test A showed that the ability of TLI to create a vortical structure and the effectiveness of these induced vortical structures in reducing the strength of the leakage vortex heavily depends on the mounting location of the TLI. Changing the mounting location from 40% to 65% axial chord resulted in a reduction of 36% FOM.

Test B: The spanwise Delta C_p distribution of passage 8, passage 10 and passage 12 is compared with reference passage (passage 14) in Fig. 18, 19 and 20. Blade 8 in test B is similar to blade 6 in test A as both had a single TLI mounted on the blade tip at 40% of axial chord. Thus, the FOM value obtained for passage 8 is 4.0

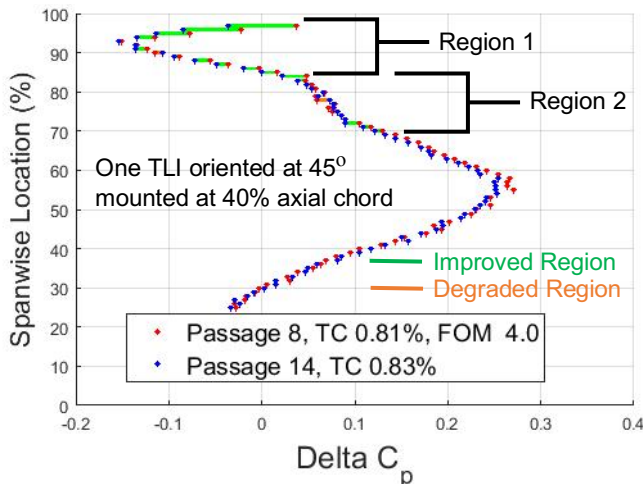


Figure 18: Spanwise distribution of Delta C_p for passage 8 with passage 14 as reference passage

close to 3.6, the FOM value of passage 6 in test A.

When the number of TLIs mounted on the blade tip is increased from one to three, the FOM of the passage slightly increased from 4 to 4.5. Comparing Fig. 18 and 19, one can see that adding two more TLIs on the blade tip reduced the losses in the region 1. However, the losses in region 2 are increased. Adding more TLIs on the blade tip introduced more TLI induced vortical structures in the flow field (as shown in Fig. 13) and was more effective in reducing the strength of the leakage vortex. Weaker leakage vortex resulted in lower loss in region 1. In region 2 the strength of the secondary vortex is increased due to weaker leakage vortex and resulted in more loss. Overall there is a slight increase in efficiency of passage 10.

A similar but more pronounced result was obtained in passage 12 where five TLIs were attached on the blade tip. Figure 20 suggests that the losses in region 1 were significantly reduced but the losses in region 2 were increased. As shown in Fig. 20 adding more TLIs onto the suction side of the blade tip increases the overall strength of the clockwise rotating TLI induced vortex, thus effectively reducing the counter clockwise rotating leakage vortex and in turn increasing the strength of the secondary vortex. The FOM obtained for passage 12 was 5.6. The tip leakage flow mitigation ability of passage 12 was increased as the reduction in losses in region 1 were greater than the generation of losses in region 2. Increasing the number of TLIs mounted on the suction side corner of the turbine blade tip has a clear benefit on region 1 of the passage. This can be seen in Fig. 18, 19 and 20, where adding TLIs onto the surface of the blade tip results in rightward shift of the Delta C_p plot. Due to this shift, the FOM values of the three test passages shows that the FOM value increases with the number of TLIs mounted. Even though addition of TLIs onto the blade tip induces losses in region 2 the overall effect of the adding the TLIs on the blade tip decreases the total loss in the flow field. It should be noted that, this study on the effect of number of TLIs mounted on leakage flow also depends on the chord wise position of the TLIs. Mounting additional TLIs near the trailing edge of the blade would have detrimental effect on leakage flow mitigation.

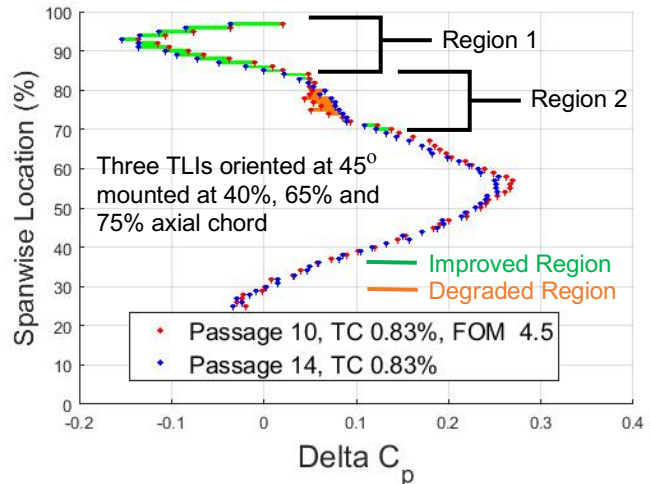


Figure 19: Spanwise distribution of Delta C_p for passage 10 with passage 14 as reference passage

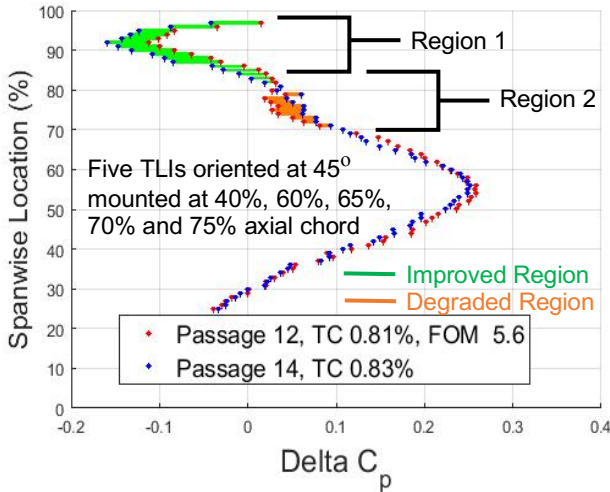


Figure 20: Spanwise distribution of Delta Cp for passage 12 with passage 14 as reference passage

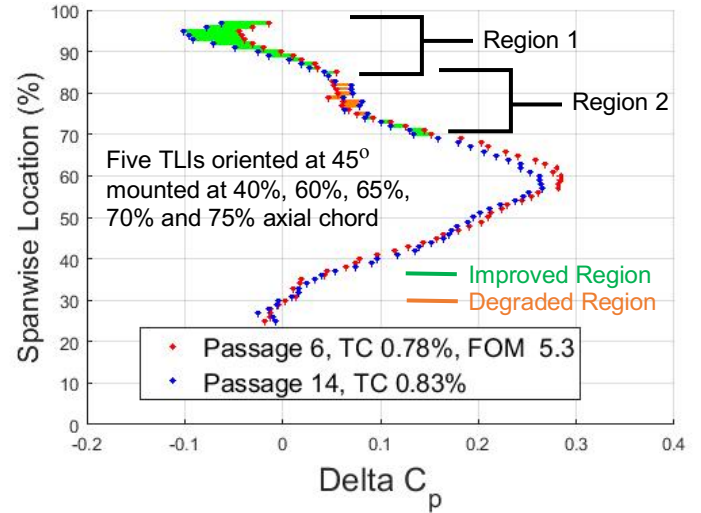


Figure 21: Spanwise distribution of Delta Cp for passage 6 with passage 14 as reference passage

Test C: Figures 21 and 22 shows spanwise variation of delta Cp for passage 6 and passage 12 with reference passage 20. Blade 6 has five TLIs attached on its blade tip and gives a FOM of 5.3, similar to FOM (5.6) of blade 12 in test B. A comparison of Fig. 21 and 22 indicates that both TLIs oriented at 45° and 135° have benefited the region 1. But the improved region for passage 12 is only from 92% to 97% of blade-span. Addition of TLIs oriented at 135° has very little effect on the flow field from 85% to 92% of blade-span (as shown in Fig. 22). In region 2 significant amount of loss is developed in passage 12. The poor performance of passage 12 is mainly because the leakage vortex is pushed towards the casing. Due to this, the interaction between the leakage vortex and secondary vortex is reduced. The effective strength of secondary vortex is increased which in turn increases the losses in region 2. Hence, overall effect of mounting a TLI at 135° is detrimental to the efficiency of the passage. The FOM of passage 12 is -5.1 indicating the significant amount of losses developed in the passage. The mounting orientation of the TLI onto the blade tip surface significantly affects the character of leakage flow mitigation in the passage.

CONCLUDING REMARKS AND FUTURE WORK

The current study is a proof of concept for the Tip Leakage Interrupter (TLI) that is a novel approach to mitigate the adverse effects of tip leakage vortical flow system. The current experimental results show that the vortex generators in the form of TLI reduce the adverse aerodynamic influence of the tip leakage flow.

The aerodynamic performance of the blades with the newly introduced TLI concept depends on the mounting location, number and orientation of the TLIs placed near the suction side corner of the tip airfoil.

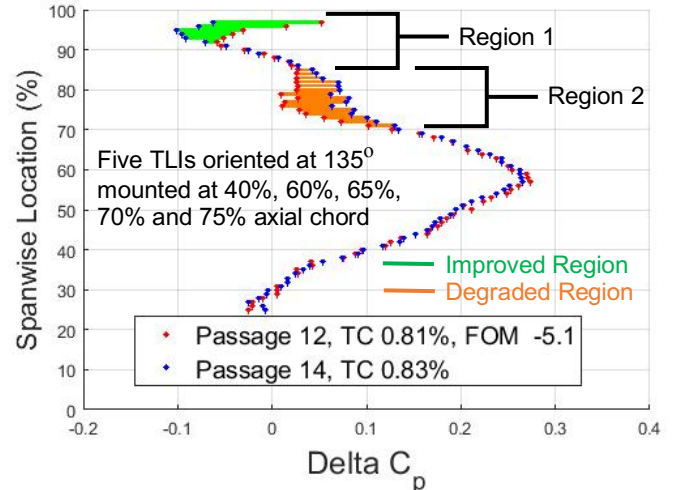


Figure 22: Spanwise distribution of Delta Cp for passage 12 with passage 14 as reference passage

The mounting location of the TLIs determines the effectiveness of the TLI in controlling the leakage flow. In a comparative experimental study of three TLI locations, it is determined that the TLI mounted at 40% of axial chord provided the best overall tip leakage control; the TLI mounted at 65% of axial chord provided moderate overall tip flow control, and the TLI mounted at 75% of axial chord adversely affected the leakage flow.

The overall effectiveness of the TLI improves when the “only” TLI is located very near the minimum pressure point (40% axial-chord). The leakage mitigation monotonically deteriorates when the TLI is moved away from the minimum pressure point towards the trailing edge.

Multiple TLIs mounted on the blade tip directly influence the aerodynamic field at the exit of the passage. Hence, mounting a greater number of TLIs on the blade tip before 75% of the axial chord would improve the tip leakage mitigation effort.

Mounting five TLIs on the blade tip (blade 12) mitigated the leakage vortex more effectively than mounting three TLIs (blade 10) or mounting one TLI on the blade tip (blade 8). In terms of FOM, blade 12 gives the best result.

The corrective effect of TLIs is accumulative up to five combined TLIs. However, caution needs to be exercised on deciding how many TLIs can be used without inducing higher aerodynamic losses especially near the aft portion of the suction side of the tip airfoil.

The mounting angle of TLIs on the blade tip plays a significant role in the attenuation of the tip leakage vortex. The TLI mounted at 45° (blade 6) creates a vortical system counteracting the leakage vortex, measurably mitigating the leakage flow. Among the two different configurations, the TLI mounted at 135° (blade 12) has adverse aerodynamic performance as it encouraged a vortical system that is enhancing the leakage flows.

This paper also benefits from a new and effective approach for the reduction of experimental errors from Dynamic Total Pressure Probe (DTP) measurements in AFTRF. By performing a subtraction from a C_p using a "reference C_p " value effectively reduces experimental error. The (ΔC_p) approach also effectively removes bias errors occurring in subsequent experiments performed on different days or the repeat experiments in the same day. The same (ΔC_p) method can also be applied in CFD efforts so that the DTP data from experiments can be easily compared to CFD predictions.

The next step in this study is to numerically analyze the turbine stage with TLI configurations for a better understanding of this interaction between the TLI induced vortex, the tip leakage vortex and passage vortex. The total-to-total efficiency changes in the turbine stage can be predicted to further study and optimize the aerodynamic benefits of the TLIs.

ACKNOWLEDGMENTS

The authors of this paper acknowledge the outstanding support of Aerospace Engineering Laboratory Staff and its IT Department. Mr. Harry Houtz and Mr. Nick Doroschenko's support for the development and implementation of the DTP probe. The experimental research greatly benefited from the early contributions of Dr. Jason Town especially for the measurement systems, data acquisition setup and data reduction procedures.

REFERENCES

1. Boyle, R. J., Haas, J. E., Katsanis, T., 1984, "Comparison between Measured Turbine Stage Performance and the Predicted Performance using Quasi-3D Flow and Boundary Layer Analyses," NASA TM-83640, presented at the 20th AIAA/ASME/SAE Joint Prop. Conf., Cincinnati, Ohio.
2. Glassman, A. J., 1973, "Turbine Design and Application," NASA SP-290.
3. Bindon, J. P., 1989, "The Measurement and Formation of Tip Clearance Loss," ASME J. of Turbomachinery, **111**, pp. 257-263, Paper No. 88-GT-203.
4. Denton, J. D., 1993, "Loss Mechanisms in Turbomachines," ASME Paper No. 93-GT-435.
5. Key, N. L., Arts, T., 2006, "Comparison of Turbine Tip Leakage Flow for Flat Tip and Squealer Tip Geometries at High-Speed Conditions," ASME J. of Turbomachinery, **128**, pp. 123-130. Paper No. 2004-GT-53979.
6. Dey, D., 2001, "Aerodynamic Tip Desensitization in Axial Flow Turbines," Ph.D. Thesis, 2001d, The Pennsylvania State University.
7. Camci, C., Dey, D., Kavurmacioglu, L. A., 2005, "Aerodynamics of Tip Leakage Flows Near Partial Squealer Rims in an Axial Flow Turbine Stage," ASME J. of Turbomachinery, **127**, (1), 14-24, doi:10.1115/1.1791279.
8. Senel, C.B., Maral, H., Kavurmacioglu, L. A., Camci, C., 2018, "An Aerothermal Study of the Influence of Squealer Width and Height near a HP Turbine Blade," International Journal of Heat and Mass Transfer, **120**, pp. 18-32.
9. Dey, D. and Camci, C., 2001, "Aerodynamic Tip Desensitization of an Axial Turbine Rotor Using Tip Platform Extensions," ASME paper 2001-GT-484.
10. Rao, N., 2005, "Desensitization of Over Tip Leakage in an Axial Turbine Rotor by Tip Surface Coolant Injection," Ph.D. Thesis, 2005d, The Pennsylvania State University.
11. Rao, N., Camci, C., 2004, "Injection from a Tip Trench as a Turbine Tip Desensitization Method – Part 1: Effect of Injection Mass Flow Rate," ASME paper GT2004-53256, ASME Turbo Expo Conference, Vienna, Austria.
12. Rao, N., Camci, C., 2004, "Injection from a Tip Trench as a Turbine Tip Desensitization Method – Part 2: Leakage Flow Sensitivity to Injection Location," ASME paper GT2004-53258, Proceedings of ASME Turbo Expo Conference, Vienna, Austria.
13. Rao, N., Gumusel, B., Kavurmacioglu, L.A., Camci, C., 2006, "Influence of Casing Roughness on the Aerodynamic Structure of Tip Vortices in an Axial Flow Turbine," ASME paper GT2006-91011, ASME Turbo Expo Conf, Barcelona, Spain.
14. Gumusel, B., 2008, "Aerodynamic and Heat Transfer Aspects of Tip and Casing Treatments Used for Turbine Tip Leakage Control," Ph.D. Thesis, 2008d, The Pennsylvania State University.
15. Kavurmacioglu, L.A., Senel, C.B., Maral, H., Camci, C., 2017, "Casing Grooves to Improve Aerodynamic Performance of a HP Turbine Blade," Aerospace Science and Technology, ISSN: 1270-9638, Elsevier, to appear in April 2018.
16. Bons, J. P., Sondergaard, R., Rivir, R. B., 2000, "Turbine Separation Control Using Pulsed Vortex Generator Jets," ASME J. of Turbomachinery, **123**, pp. 198-206, Paper No. 2000-GT-262.

17. Gokce, Z. O., Camci, C., 2011, "Unsteady Flow Characteristics and Viscous Flow Losses Behind Multiple Rows of Circular Pin Fins in Coolant Channels," ASME/IMECE paper IMECE 2011-64333, Denver, Colorado, USA.
18. Beeck, A. R., Brown, G. E., 2010, "Turbine Blade Tip with Vortex Generators," U.S. Patent # 8,690,536, September, 2010.
19. Xiao, X., McCarter, A., Lakshminarayana, B., 2000, "Tip Clearance Effects in a Turbine Rotor: Part 1- Pressure Field and Loss," ASME Paper No. 2000-GT-476.
20. McCarter, A., Xiao, X., Lakshminarayana, B., 2000, "Tip Clearance Effects in a Turbine Rotor: Part 2- Velocity Field and Flow Physics," ASME Paper No. 2000-GT-477.
21. Lakshminarayana, B., Camci, C., Halliwell, I., Zaccaria, M., 1996, "Design, Development, and Prediction of a Turbine Research Facility to Study Rotor Stator Interaction Effects," Int. Journal of Turbo and Jet Engines, **13**, pp. 155-172.
22. Town, J., Akturk, A., Camci, C., 2012, "Total Pressure Correction of a Sub-Miniature Five-Hole Probe in Areas of Pressure Gradients," ASME Paper No. GT2012-69280, pp. 855-861.
23. Town, J., Camci, C., 2015, "A Time Efficient Adaptive Gridding Approach and Improved Calibrations in Five Hole Probe Measurements," Int. Journal of Rotating Machinery, International J. of Rotating Machinery, Vol. 2015, Article ID 376967.
24. Town, J., 2015, "An Investigation of Rim Seal/Disk Cavity Flow and it's Interaction with High Pressure Turbine Rotor Flows," Ph.D. Thesis, 2015d, The Pennsylvania State University.
25. Kline, S. J., McClintock, F. A., 1953, "Describing Uncertainties in Single-Sample Experiments," Mechanical Engineering, **75**, pp. 3-8.